JACS
JOURNAL OF THE AMERICAN CHEMICAL SOCIETY

Communication

pubs.acs.org/JACS

The Room-Temperature Superionic Conductivity of Silver Iodide Nanoparticles under Pressure

Takayuki Yamamoto,[†] Mitsuhiko Maesato,*[,†] Naohisa Hirao,[‡] Saori I. Kawaguchi,[‡] Shogo Kawaguchi,[‡] Yasuo Ohishi,[‡] Yoshiki Kubota,[§] Hirokazu Kobayashi,[†,∥] and Hiroshi Kitagawa*[,†,⊥,#]

[†]Division of Chemistry, Graduate School of Science, Kyoto University, Kitashirakawa-Oiwakecho, Sakyo-ku, Kyoto 606-8502, Japan
[‡]Japan Synchrotron Radiation Research Institute (JASRI), SPring-8, 1-1-1 Kouto, Sayo-cho, Sayo-gun, Hyogo 679-5148, Japan
[§]Depertment of Physical Science, Graduate School of Science, Osaka Prefecture University, Sakai, Osaka 599-8531, Japan
[∥]PRESTO, Japan Science and Technology Agency (JST), 4-1-8 Honcho, Kawaguchi, Saitama 332-0012, Japan
[⊥]Institute for Integrated Cell-Material Sciences (iCeMS), Kyoto University, Yoshida, Sakyo-ku, Kyoto 606-8501, Japan
[#]INAMORI Frontier Research Center, Kyushu University, 744 Motooka, Nishi-ku, Fukuoka 819-0395, Japan

Supporting Information

ABSTRACT: We performed variable-temperature synchrotron powder X-ray diffraction measurements and impedance spectroscopy under pressure for silver iodide (AgI) nanoparticles with a diameter of 11 nm. The superionic conducting α-phase of AgI nanoparticles was successfully stabilized down to at least 20 °C by applying a pressure of 0.18 GPa, whereas the transition temperature was 147 °C in bulk AgI at ambient pressure. To our knowledge, this is the first example of the α-phase of AgI existing stably at room temperature.

Recently, enhancement of the performance and safety of batteries has been highlighted due to the widespread use of mobile electronic devices. Liquid electrolytes are commonly used for batteries at present, but safety problems such as liquid spill and ignition exist. To overcome these problems, all-solid-state batteries have been actively studied.[1−4] Silver iodide (AgI) has attracted much attention as an ionic conductor in solid electrolytes. Bulk AgI consists of the β-phase with wurtzite structure and the γ-phase with zincblende structure at ambient temperatures and pressures.[5,6] Above 147 °C, the β/γ-phases change to the α-phase, which shows very high Ag^+ conductivity of more than 1 S/cm originating from sublattice melting of Ag^+.[7,8] To stabilize the α-phase down to lower temperature, various methods have been attempted so far, such as chemical substitution,[9−12] embedding in a glass matrix,[13−16] applying pressure,[17−20] and downsizing.[21−24] It is known that the hysteresis of the transition temperatures in the heating and cooling processes becomes larger with decreasing particle size of AgI.[23,24] For AgI nanoparticles with a diameter of 11 nm, the transition temperature from the α-phase to the β/γ-phases is 40 °C, showing a large hysteresis of more than 100 °C,[24] although the hysteresis is only 2.5 °C in bulk AgI.[25] AgI is used for cloud seeding because of its similar crystal structure to ice.[26] It is well-known that the melting point of ice shifts to lower temperature on applying moderate pressure due to the lower density of ice than that of water.[27] In bulk AgI, similar to ice, it has been reported that the transition temperature decreases under pressure.[17−20] However, there is no study on the effect of pressure on AgI nanoparticles. Here, we report the stabilization of the α-phase down to room temperature by applying pressure to AgI nanoparticles.

The AgI nanoparticles used in this work were prepared by liquid-phase synthesis, as in the previous report,[24] and characterized by transmission electron microscopy (TEM) and powder X-ray diffraction (PXRD). Monodispersed nanoparticles were observed using TEM, and their mean diameter and size distribution were estimated to be 11.4 ± 4.5 nm (Figure 1a and 1b). A PXRD pattern of the as-synthesized AgI nanoparticles clearly showed that they consisted of β/γ-phases

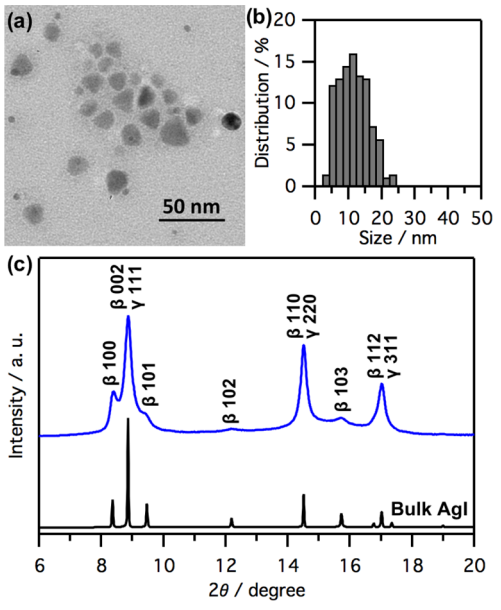

Figure 1. (a) TEM image and (b) size distribution of AgI nanoparticles. (c) PXRD patterns of the as-synthesized AgI nanoparticles (blue) and bulk (black) at ambient temperatures and pressures.

Received: November 2, 2016
Published: January 17, 2017

DOI: 10.1021/jacs.6b11379
J. Am. Chem. Soc. 2017, 139, 1392−1395

at ambient temperatures and pressures (Figure 1c). Moreover, the crystal size of the AgI nanoparticles calculated using the Scherrer equation (13.4 and 10.2 nm for β- and γ-phases, respectively) was consistent with the mean diameter determined by TEM observation.

To investigate the phase-transition behavior of AgI nanoparticles, we performed variable-temperature synchrotron PXRD measurements under ambient pressure at SPring-8 BL02B2 (Figure S1). Upon heating, the as-synthesized β/γ-phases gradually changed to the α-phase between 150 and 190 °C, and a small amount of the α-phase remained at 30 °C on subsequent cooling at ambient pressure. Figure 2a shows the

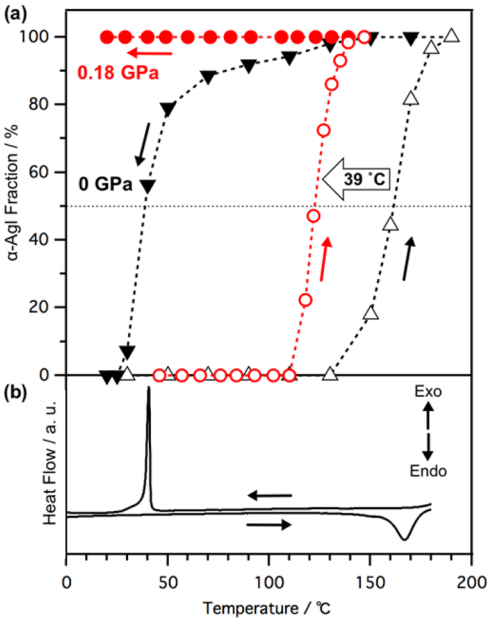

Figure 2. (a) Temperature dependence of the α-phase AgI fractions under 0.18 GPa (circles) and at ambient pressure (triangles). Open and closed symbols are for the heating and cooling processes, respectively. (b) DSC thermograms of AgI nanoparticles at ambient pressure.

temperature dependence of the fraction of the α-phase calculated by Rietveld refinement on the PXRD patterns. The transition temperatures during the heating and cooling processes are 162 and 39 °C, respectively, where the transition temperature is defined as the temperature at which the fraction of the α-phase reaches 50%. The results are in good agreement with those of differential scanning calorimetry (DSC), as shown in Figure 2b.

Next, the phase-transition behavior of AgI nanoparticles under pressure was investigated using variable-temperature synchrotron PXRD measurements under pressure at SPring-8 BL10XU (Figure 3). AgI nanoparticles were loaded into a diamond anvil cell with sodium chloride as the pressure transmitting medium and pressure marker,[28] and the cell was heated with an electric resistance heater. The pressure was controlled using a gas membrane and adjusted at each temperature. Upon heating under 0.18 GPa, a gradual phase transition from the β/γ-phases to the α-phase occurred between 110 and 147 °C, which was a lower temperature than at ambient pressure (Figure S1). Upon cooling, in contrast, the diffraction patterns did not change and only the α-phase was observed even at 20 °C under 0.18 GPa, indicating

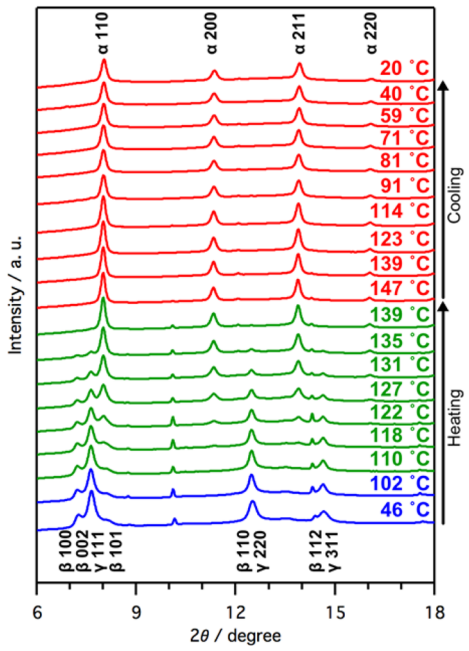

Figure 3. Variable-temperature synchrotron PXRD patterns under 0.18 GPa for AgI nanoparticles. Blue and red curves denote PXRD patterns containing only the β/γ-phases and α-phase, respectively. Green curves denote a mixture of these phases.

the first observation of α-phase AgI at room temperature. The crystal size of the α-phase was calculated as 18.0 nm using the Scherrer equation, and it was confirmed that obvious crystal size growth did not occur during the thermal cycle.

For further detailed analysis, as for the ambient-pressure data, we calculated the fraction of α-phase at each temperature from Rietveld refinement on synchrotron PXRD patterns and plotted it against temperature in Figure 2a. The transition temperature upon heating is estimated to be 123 °C under 0.18 GPa, which is lower than that under ambient pressure by 39 °C (Figure 4, yellow squares and dotted line). Unfortunately, we could not perform synchrotron PXRD measurements below room temperature due to a technical limitation, so the transition

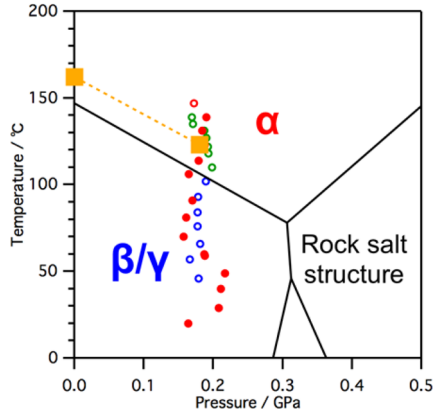

Figure 4. Pressure–temperature phase diagram of bulk AgI from the literature[19] (black) and measurement points of variable-temperature synchrotron PXRD measurements in this work (circles: open, heating; closed, cooling). Red, green, and blue colors correspond to the diffraction patterns of AgI nanoparticles in Figure 3. Yellow squares denote transition temperatures upon heating, determined using Rietveld refinement.

DOI: 10.1021/jacs.6b11379
J. Am. Chem. Soc. 2017, 139, 1392–1395

temperature upon cooling under 0.18 GPa could not be determined. According to the phase diagram of bulk AgI (Figure 4, black line), the transition temperature decreased by 41 °C under 0.18 GPa, and this is consistent with our nanoparticles case. So we can conclude that stabilization of the α-phase at room temperature under pressure observed in AgI nanoparticles originates from both size and pressure effects.

To investigate the ionic conductivity of AgI nanoparticles, we performed AC impedance spectroscopy under ambient pressure and 0.20 GPa. AgI nanoparticles were loaded into a piston cylinder cell with Daphne Oil 7373 as the pressure-transmitting medium and manganin wire as the pressure marker.[29] Pressure was applied at room temperature and clamped before the thermal cycle. Typical Nyquist plots are shown in Figure S6, and by fitting the arc with a semicircle, the ionic conductivity was determined at each temperature (Figure 5). Upon heating under ambient pressure, the ionic

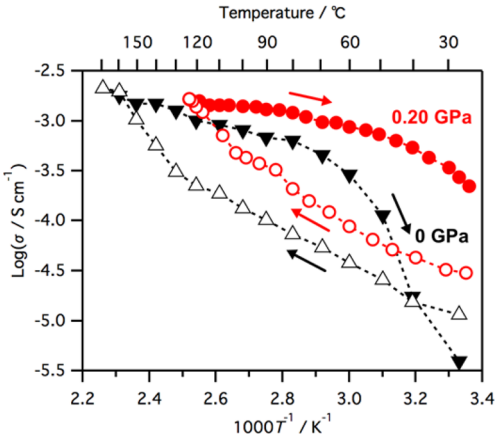

Figure 5. Temperature dependence of ionic conductivity for AgI nanoparticles under 0.20 GPa (circles) and at ambient pressure (triangles). Open and closed symbols are for the heating and cooling processes, respectively.

conductivity increased gradually. Above 130 °C, a noticeable change was observed, associated with a phase transition from the β/γ-phases to the α-phase. Upon cooling, on the other hand, the ionic conductivity showed a higher value than upon heating, and a sudden drop was observed at 40 °C due to the disappearance of the α-phase. Under 0.20 GPa, in contrast, high ionic conductivity was retained down to a lower temperature, which suggests stabilization of the α-phase due to the effect of pressure. The reason why ionic conductivity starts to drop at room temperature during the cooling process could be a partial phase transition from the α-phase to the β/γ-phases due to a small pressure leak during the thermal cycle.

The ionic conductivity of the AgI nanoparticles was 2.1×10^{-3} S/cm at 169 °C under ambient pressure, which was lower than the previously reported value.[23] This could originate from the amount of the protecting polymer and/or vacancies.

The change in transition temperature induced by applying pressure can be explained using the Clausius–Clapeyron equation:

$$\frac{dT}{dP} = \frac{T\Delta V}{\Delta H}$$

where T, P, ΔV, and ΔH denote temperature, pressure, volume change, and transition enthalpy, respectively. As mentioned above, the melting point of ice decreases under pressure due to volume shrinkage during melting. In AgI, as is the case with ice, considering that the density of the α-phase is higher than that of the β/γ-phases ($\Delta V < 0$) and that the phase transition from the β/γ-phases to the α-phase is endothermic ($\Delta H > 0$), we can expect that the transition temperature decreases on applying pressure. We evaluate $T = 435$ K and $\Delta V = 2.6 \times 10^{-6}$ m^3/mol from variable-temperature synchrotron PXRD measurement and $\Delta H = 3.9$ kJ/mol from DSC, and then $T\Delta V/\Delta H = -2.9 \times 10^{-7}$ K/Pa at ambient pressure for AgI nanoparticles. This value is consistent with the observed $dT/dP = -2.2 \times 10^{-7}$ K/Pa (Figure 4, yellow dotted line) and previous reports of -1.5×10^{-7} K/Pa for bulk AgI.[30,31]

In summary, we investigated the pressure effect on AgI nanoparticles' phase-transition behavior and ionic conductivity using variable-temperature synchrotron PXRD measurements and AC impedance spectroscopy under pressure. The α-phase was stabilized down to 20 °C by applying a pressure of 0.18 GPa to AgI nanoparticles with a diameter of 11 nm, as a result of the combination of pressure and size effects.

■ ASSOCIATED CONTENT

Supporting Information

The Supporting Information is available free of charge on the ACS Publications website at DOI: 10.1021/jacs.6b11379.

Experimental details, variable-temperature synchrotron PXRD patterns, Rietveld refinement, and Nyquist plots (PDF)

■ AUTHOR INFORMATION

Corresponding Authors

*maesato@kuchem.kyoto-u.ac.jp
*kitagawa@kuchem.kyoto-u.ac.jp

ORCID

Hiroshi Kitagawa: 0000-0001-6955-3015

Notes

The authors declare no competing financial interest.

■ ACKNOWLEDGMENTS

This work was supported by Core Research for Evolutional Science and Technology (CREST) and ACCEL from the Japan Science and Technology Agency (JST), and Grants-in-Aid for JSPS Fellows (27-1603) from the Japan Society for the Promotion of Science (JSPS). Synchrotron XRD measurements were supported by the Japan Synchrotron Radiation Research Institute (JASRI) (Proposal Nos. 2014B1783, 2015A1835, 2015B1701, and 2016A1661).

■ REFERENCES

(1) Owens, B. B. *J. Power Sources* **2000**, *90*, 2–8.
(2) Armand, M.; Tarascon, J. M. *Nature* **2008**, *451*, 652–657.
(3) Simon, P.; Gogotsi, Y. *Nat. Mater.* **2008**, *7*, 845–854.
(4) Kato, Y.; Hori, S.; Saito, T.; Suzuki, K.; Hirayama, M.; Mitsui, A.; Yonemura, M.; Iba, H.; Kanno, R. *Nat. Energy* **2016**, *1*, 16030.
(5) Burley, G. *J. Chem. Phys.* **1963**, *38*, 2807–2812.
(6) Takahashi, T.; Kuwabara, K.; Yamamoto, O. *J. Electrochem. Soc.* **1969**, *116*, 357–360.
(7) Tubandt, C.; Lorenz, F. *Z. Phys. Chem.* **1914**, *87*, 543.
(8) Hull, S. *Rep. Prog. Phys.* **2004**, *67*, 1233–1314.
(9) Bradley, J. N.; Greene, P. D. *Trans. Faraday Soc.* **1967**, *63*, 424–430.
(10) Shahi, K.; Wagner, J. B., Jr. *J. Phys. Chem. Solids* **1982**, *43*, 713–722.

DOI: 10.1021/jacs.6b11379
J. Am. Chem. Soc. 2017, 139, 1392–1395

(11) Kumar, P. S.; Balaya, P.; Goyal, P. S.; Sunandana, C. S. *J. Phys. Chem. Solids* **2003**, *64*, 961−966.
(12) Mohan, B. D.; Sunandana, C. S. *J. Phys. Chem. Solids* **2004**, *65*, 1669−1677.
(13) Tatsumisago, M.; Shinkuma, Y.; Minami, T. *Nature* **1991**, *354*, 217.
(14) Saito, T.; Tatsumisago, M.; Torata, N.; Minami, T. *Solid State Ionics* **1995**, *79*, 279−283.
(15) Lee, J. S.; Adams, S.; Maier, J. *J. Electrochem. Soc.* **2000**, *147*, 2407−2418.
(16) Foltyn, M.; Wasiucionek, M.; Garbarczyk, J.; Nowinski, J. L. *Solid State Ionics* **2005**, *176*, 2137−2140.
(17) Davis, B. L.; Adams, L. H. *Science* **1964**, *146*, 519−521.
(18) Bassett, W. A.; Takahashi, T. *Am. Mineral.* **1965**, *50*, 1576−1594.
(19) Mellander, B. E.; Bowling, J. E.; Baranowski, B. *Phys. Scr.* **1980**, *22*, 541.
(20) Mellander, B. E. *Phys. Rev. B: Condens. Matter Mater. Phys.* **1982**, *26*, 5886−5896.
(21) Guo, Y. G.; Lee, J. S.; Maier, J. *Solid State Ionics* **2006**, *177*, 2467−2471.
(22) Liang, C.; Terabe, K.; Hasegawa, T.; Aono, M.; Iyi, N. *J. Appl. Phys.* **2007**, *10*, 1924308.
(23) Makiura, R.; Yonemura, T.; Yamada, T.; Yamauchi, M.; Ikeda, R.; Kitagawa, H.; Kato, K.; Takata, M. *Nat. Mater.* **2009**, *8*, 476−480.
(24) Yamasaki, S.; Yamada, T.; Kobayashi, H.; Kitagawa, H. *Chem. - Asian J.* **2013**, *8*, 73−75.
(25) Binner, J. G. P.; Dimitrakis, G.; Price, D. M.; Reading, M.; Vaidhyanathan, B. *J. Therm. Anal. Calorim.* **2006**, *84*, 409−412.
(26) Marcolli, C.; Nagare, B.; Welti, A.; Lohmann, U. *Atmos. Chem. Phys.* **2016**, *16*, 8915−8937.
(27) Bridgman, P. W. *Proc. Am. Acad. Arts Sci.* **1912**, *47*, 441−558.
(28) Matsui, M.; Higo, Y.; Okamoto, Y.; Irifune, T.; Funakoshi, K. *Am. Mineral.* **2012**, *97*, 1670−1675.
(29) Zeto, R. J.; Vanfleet, H. B. *J. Appl. Phys.* **1969**, *40*, 2227−2231.
(30) Bridgman, P. W. *Proc. Am. Acad. Arts Sci.* **1915**, *51*, 55−124.
(31) Mellander, B. E.; Baranowski, B.; Lunden, A. *Phys. Rev. B: Condens. Matter Mater. Phys.* **1981**, *23*, 3770−3773.

DOI: 10.1021/jacs.6b11379
J. Am. Chem. Soc. 2017, 139, 1392−1395